Numerical Modelling of GaAs/AlGaAs Heterojunctions
and GaAs/AlGaAs Heterojunction Bipolar Transistors

P.A.MAWBY, C.M.SNOWDEN, D.V.MORGAN[†]

Dept. of Electrical and Electronic Engineering
University of Leeds, Leeds.

† UWIST, Cardiff, Wales

ABSTRACT

This paper describes a computer modelling system for use
in the study of these GaAs/AlGaAs heterostructure devices.
The model is based on the solution of the basic device
equations, which are solved using the finite - difference
technique, and results are given for both the one dimensional
and two dimensional cases. These results show that suitable
grading of the emmiter base junction is important in the
optimum design of the device.

INTRODUCTION.

With the advent of recent epitaxial techniques (MBE and
MOCVD), it has become possible to introduce an extra degree of
freedom into the design of semiconductor devices. It is now
possible to engineer the band-gap of the device, allowing a
flexibility hitherto unattainable in conventional device
design. By careful control of band-gap and doping, it is
possible to control the injection or confinement of electrons
and holes. It is this which has paved the way for many of the
new GaAs devices currently being developed.

The essence of heterojunction bipolar transistors is the
confinement of holes to the base region. Changing the
composition at the emitter-base junction, from AlGaAs in the
emitter, to GaAs in the base, sets up an adverse "quasi-
electric" potential barrier that prevents hole injection into
the emitter. As holes can no longer be injected from the

base, it is not necessary to have an emitter that is more heavily doped than the base region, in order to obtain a reasonable injection ratio (γ). Two of the main time delays in the bipolar transistor are the junction charging times, these are RC time constants, so lowering the resistance will improve the maximum frequency of oscillation f_{max}. Increased base doping, considerably reduces both the base resistance, and the emitter depletion capacitance. Sufficient reduction of these two elements will increase the frequency range into the millimetre wave area, and theoretical calculations have predicted cut-off frequencies f_t, of over 100 GHz [1].

Recently reported results have shown HBT's to have enormous promise in the fields of high speed digital I.C.'s [2], MMIC's [3] and also in opto-electronics as a phototransistor [4]. Particularly attractive is the development of ECL circuits which have already shown themselves to be the fastest silicon digital technology with f_t's of nearly 10 GHz.

In this paper, a simulation of the HBT, using the finite-difference technique, is discussed. A one-dimensional simulation has been used to examine the effects of base-emitter compositional grading, on the current transport mechanisms at this junction. Conclusions drawn from this study have been implemented in a two-dimensional model of the HBT in order to determine the optimum emitter mole-fraction and grading profile.

PROBLEM FORMULATION.

The basic "phenomenological" device equations for semiconductors used in device simulation work are [5] :-

$$\nabla.(\epsilon \vec{E}) = q (\Gamma - n + p)$$ (1)

where : $\Gamma = N_D - N_A$

$$\frac{dn}{dt} = \frac{1}{q} \nabla.\vec{J}_n - U$$ (2)

$$\frac{dp}{dt} = \frac{1}{q} \nabla.\vec{J}_p - U$$ (3)

Equation (1) is Poisson's equation relating electric field to enclosed charge. Equations (2) and (3) are the current continuity equations for electrons and holes, and they are a statement of the conservation of charge. These equations are general, and form a set of coupled partial differential equations.

In a device of non-uniform composition the basic device equations must be modified in order to take account the non-

uniformity of the material parameters. The assumption that the permittivity is uniform can now no longer be taken to apply. In silicon device simulations where band-gap narrowing is considered this variation is ignored, although it can be very important. In the present non-uniform device Poisson's equation is modified to :-

$$\nabla \epsilon . \vec{E} \ + \ \epsilon \nabla . \vec{E} \ = \ q \ (\ \Gamma - n + p \ ) \tag{4}$$

This simplifies when the device is of uniform composition ($\nabla \epsilon = 0$) to the familiar form of Poisson's equation.

The classical Shockley equations for current density [6] must be extended to include extra terms. These take into account the internal "quasi-electric" fields due to the positional dependence of the band-gap, and "quasi-diffusion" due to the positional dependence of the density of states [7]. For a semiconductor at a constant temperature the particle current densities are given by [6] :

$$\vec{J}_n \ = \ - n\mu_n \nabla E_{fn} \tag{5}$$

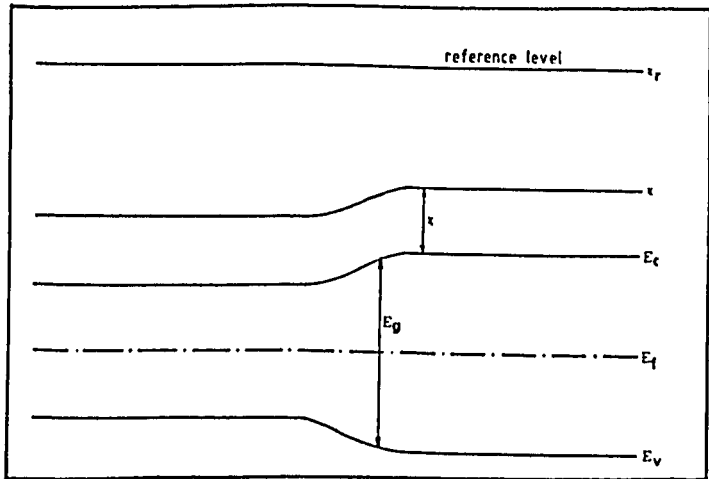$$\vec{J}_p \ = \ - p\mu_p \nabla E_{fp} \tag{6}$$

Figure 1.

Generalised Energy-band diagram of a non-uniform semiconductor.

from figure .1 the electron and hole Fermi-energies are given by :

$$E_{fn} \ = \ - q\psi - (\ \chi - \chi_r \ ) + kT \exp \frac{n}{N_c} \tag{7}$$

$$E_{fp} \ = \ - q\psi - (\ \chi - \chi_r \ ) + E_g + kT \exp \frac{p}{N_v} \tag{8}$$

where : χ_r is a reference energy level, ψ is the electrostatic potential, χ is the electron affinity, E_g is the material bandgap, n and p are the carrier concentrations and N_c and N_v are the conduction and valence band density of states.

Substituting equations (7) and (8) into (5) and (6) yields the following equations :-

$$\vec{J}_n = \mu_n (q\vec{E} - \nabla\chi + \frac{kT}{n}\nabla n - \frac{kT}{N_c}\nabla N_c) \qquad (9)$$

$$\vec{J}_p = \mu_p (q\vec{E} - \nabla\chi - \nabla E_g - \frac{kT}{p}\nabla p + \frac{kT}{N_v}\nabla N_v) \qquad (10)$$

Equations (9) and (10) again simplify to the familiar equation for current densities when the material is homogeneous. Equations (2) - (10) completely describe the system, subject to the appropriate boundary conditions. In order to arrive at these equations the following assumptions have been made :-

(i)   All impurity atoms are completely ionised

(ii)   Position dependent effective mass is still a valid concept

(iii) Anderson electron affinity rule applies

(iv)   No interfacial charge exists at the heterojunction due to lattice mismatch

(v)   Doping is sufficiently low to avoid degeneracy

(vi)   Boltzmann statistics are taken to apply

(vii) Band-gap narrowing does not occur

(viii) Minority carrier mobilities are the same as for majority carriers

Points (ii) and (iii) assume that grading is "sufficiently gradual" [7] this is implicit in equations (5) and (6). Lundstrom and Schulke [8] have added an extra term into these equations to model the influence of Fermi-Dirac statistics on the Einstein relationship, this term is zero in the limit of condition (v).

PHYSICAL PARAMETERS

Those parameters (defined in fig.1) relating to the band structure, are based of the results of Dingle [8], who derived the following relationship:

$$\Delta E_c \; = \; 0.85 \; \Delta E_g \quad eV \tag{11}$$

$$\Delta E_v \; = \; 0.15 \; \Delta E_g \quad eV \tag{12}$$

Known as Dingles rule, this is a subject of much controversy, with more recent measurements pointing towards 50% of the discontinuity occurring in each band [9], however in this work (11) and (12) have been used. The variation of the band-gap E_g, at 300K is taken to be [10] :

$$E_g(x) \; = \; 1.422 + 1.25x \quad eV \tag{13}$$

where x < 0.4 since only mole-fractions less than the direct-indirect cross over point (approximately x = 0.45) are of interest. The compositional dependence of the density of states in the conduction and valence bands are [10] :

$$N_c(x) \; = \; (0.067 + 0.083)^{3/2} * 2.5x10^{19} \quad cm^{-3} \tag{14}$$

$$N_v(x) \; = \; (0.480 + 0.310)^{3/2} * 2.5x10^{19} \quad cm^{-3} \tag{15}$$

also the variation of the electron affinity is given by :

$$\chi(x) \; = \; 4.07 - 1.06x \quad eV \tag{16}$$

The net recombination rate is assumed to be given by a simplified Shockley - Hall - Read model in which the traps are located at band centre, and both carrier types have the same lifetime $\tau = 1ns$. Experimental results have shown this to be a reasonable choice. The expression used is :

$$U \; = \; \frac{np - n_i^2}{\tau(n+p+2n_i)} \tag{17}$$

Hole mobility is taken to be independent of the mole-fraction of aluminium in the alloy. This is reasonable since holes contribute only slightly to the overall performance of the device. However, the hole mobility - field dependence is taken into account, as well as dependence on temperature and absolute doping, resulting in the familiar expression for low field mobility :

$$\mu_{low} \; = \; \mu_o + \frac{\mu_1}{1 + \left(\dfrac{N_D + N_A}{N_{ref}}\right)^\alpha} \quad cm^2/V.s \tag{18}$$

temperature dependence is incorporated by :

$$\mu'_{low}(T,N_D+N_A) \; = \; \frac{300\mu_{low}}{T} \quad cm^2/V.s \tag{19}$$

The values of these parameters are taken from reference [11] to be $\mu_o = 50 cm^2/V.s$, $\mu_1 = 330 cm^2/V.s$, $N_{ref} = 3.232x10^{17} cm^{-3}$ and $\alpha = 0.4956$. Moreover, the field dependence is given by :

$$\mu_p(T,E,N_D+N_A) \quad = \quad \frac{\mu'_{low}}{1 + \frac{\mu'_{low}E}{v_{sat}}} \tag{20}$$

v_{sat} is the carrier saturation velocity, and for holes in GaAs, it is 1.5×10^7 cm/s. A similar relationship exists for electron mobility, the dependency on field is described by Freeman and Hobsons empirical relationship [12], giving for GaAs :
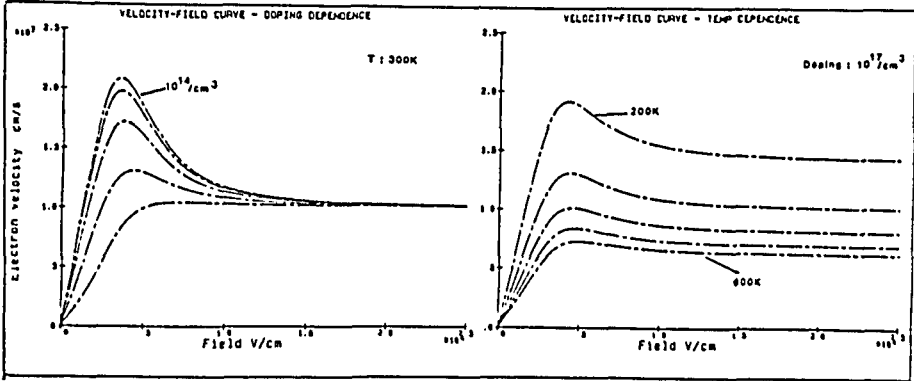

Figure 2.

Velocity field characteristics of GaAs as a
function of temperature and doping.

$$v = v(E,T,N_A+N_B) =$$

$$\frac{300\mu_{low}E}{T} \quad \frac{1 + \frac{8.5 \times 10^6 \ E^3}{\mu_{low}E_{crit}^4 \ (1 - 5.3 \times 10^{-4}T)}}{1 + \left[\frac{E}{E_{crit}}\right]^4} \quad cm^2 V^{-1} s^{-1} \tag{21}$$

where

$$E_{crit} = 4 \times 10^3 V cm^{-1}$$

with

$$\mu_{low} = \frac{8 \times 10^3}{1 + \left[\frac{N_A+N_B}{10^{17}}\right]^{0.5}} \quad cm^2 V^{-1} s^{-1} \tag{22}$$

In the alloy AlGaAs, the mobility is reduced as the mole-fraction of aluminium (x), is increased from zero, due to alloy scattering. This is included into the model empirically by scaling the low - field, room temperature value of mobility so that :

$$\mu_{RT}(x) = m(x) \cdot \mu_{RT}(0) \tag{23}$$

m(x) is a monotonically decreasing function of the mole-fraction x. As the relationship between electron mobility and mole-fraction is not at all well documented it is hoped that this approximation exhibits the correct behaviour, to a first order at least.

FINITE - DIFFERENCE APPROACH

The device is simulated over a rectangular domain, this is ideally suited to the planar device structure presently under consideration. Within the simulation domain, the grid spacings are perfectly general. Initially a coarse grid is generated which depends on doping levels and the positioning of geometric features. The mesh is then refined in those areas where large gradients of potential or carrier profile arise, in order to minimise the error in these areas (see figure 8). The solution of the device equations (2) - (4) are in terms of the three dependent variables ψ, n, p. Potential is scaled in units of thermal - volts to reduce repetitive calculations, whereas the carrier concentrations remain unscaled.

Poisson's equation is expressed using the usual "five point formula" based on the central difference Taylor expansion figure 3.

$$\frac{d(\epsilon E)}{dx}\bigg|_{i,j} = \epsilon_{i,j} \frac{\left[\frac{\psi_{i+1,j} - \psi_{i,j}}{h_i} - \frac{\psi_{i,j} - \psi_{i-1,j}}{h_{i-1}} \right]}{\frac{h_i + h_{i-1}}{2}}$$

$$+ \frac{\epsilon_{i+1,j} - \epsilon_{i-1,j}}{h_i + h_{i-1}} \frac{\psi_{i+1,j} - \psi_{i-1,j}}{h_i + h_{i-1}} + O(h^2) \tag{24}$$

As seen from figure 3, i and j refer to the node index, ϵ is the dielectric permittivity, ψ is the discretised electrostatic potential and h is the node spacing ($h_i = x_{i+1} - x_i$), an analogous expression can be written for the derivative in the y direction. If the expressions for the derivatives (24) are substituted for both directions, then an equation for $\psi_{i,j}$ can be expressed in terms of the four
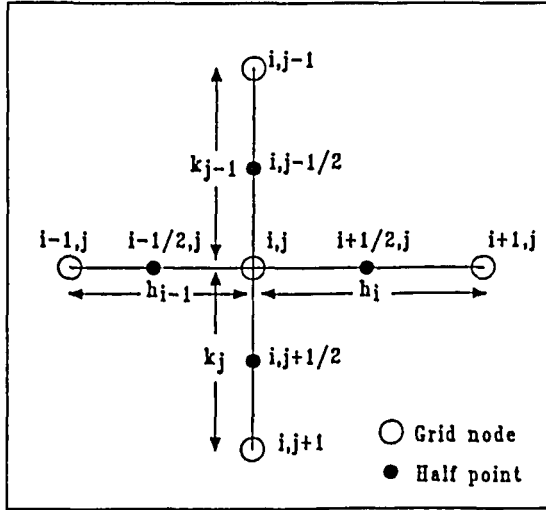
Figure 3.

Internal node on device plane, showing separations.

surrounding nodes, when this is carried out at every inner node, a system of linear simultaneous equations are obtained.

$$[A][\psi] = [B] \tag{25}$$

here $[A]$ is the coefficient matrix, $[\psi]$ is the unknown vector and $[B]$ is a known vector containing the right hand side of equation (4). The coefficient matrix $[A]$ for boundary value problems, is a sparse banded matrix, and so the solution of (25) is best arrived at iteratively for a large system of equations. The solution of Poisson's equation is obtained by using the successive over relaxation scheme (SOR) on the Gauss-Siedel method. The method is more efficient than direct methods, as the memory requirements are minimal, also round off errors are limited to the *last* iteration.

The current continuity equations (2) and (3) are second order parabolic differential equations in n and p. The current density equations are formulated in terms of the Scharfetter - Gummel equation. Because of the compositional dependence in the HBT, two parameters θ_n and θ_p are introduced, these come directly from equations (9) and (10) :

$$\vec{J}_n = q\mu_n n\nabla(\psi+\theta_n)+qD_n\nabla n \tag{26}$$

$$\vec{J}_p = q\mu_p p\nabla(\psi-\theta_p)-qD_p\nabla p \tag{27}$$

where

$$\theta_n = \frac{(\chi-\chi_r)}{q} + \frac{kT}{q}\ell n\left(\frac{N_c}{N_{cr}}\right) \tag{28}$$

$$\theta_p \ = \ -\frac{(x-x_r)}{q} \ - \ \frac{(E_g-E_{gr})}{q} \ + \ \frac{kT}{q}\ell n\left(\frac{N_v}{N_{vr}}\right) \tag{29}$$

x_r is defined such that $\theta_n \ = \ \theta_p \ = \ 0.0$ when the mole-fraction x $=0.0$. The modified equations for the current density are now used in the standard Scharfetter - Gummel equation for the current density at the "half node" points, figure 3. This method is superior to the linear approximations used in previous work, in that the potential difference between nodes is no longer a stability criterion, and allows larger space steps (h_i and k_j) to be used. Explicit schemes for the solution of equations (2) and (3) in terms of the variables n and p, using a forward difference in time may become unstable, and have very strict convergence criteria

$$\Delta t \ < \ \frac{\Delta x^2}{4D} \tag{30}$$

Equation (30) is defined for a uniform mesh, where D is the diffusion constant. For stability this condition is applied to electrons as $D_n > D_p$. Using an implicit scheme based on the Crank - Nicholson method, this restriction can be overcome. The implicit scheme is essentially a central difference in time, and is stable for all time steps. The finite - difference approximation to (2) and (3) then becomes :

$$\frac{n^{k+1}_{i,j} - n^k_{i,j}}{\Delta t} \ = \ \frac{1}{2q}\left[\nabla.\vec{J}_{n_{i,j}}^{\ k+1} + \nabla.\vec{J}_{n_{i,j}}^{\ k}\right] - U_{i,j} \tag{31}$$

$$\frac{p^{k+1}_{i,j} - p^k_{i,j}}{\Delta t} \ = \ \frac{-1}{2q}\left[\nabla.\vec{J}_{p_{i,j}}^{\ k+1} + \nabla.\vec{J}_{p_{i,j}}^{\ k}\right] - U_{i,j} \tag{32}$$

where

$$\nabla.\vec{J}_{i,j} \ = \ \frac{\vec{J}_{x_{i+1/2,j}} - \vec{J}_{x_{i-1/2,j}}}{\frac{h_i+h_{i-1}}{2}} + \frac{\vec{J}_{y_{i,j+1/2}} - \vec{J}_{y_{i,j-1/2}}}{\frac{k_j+k_{j-1}}{2}} \tag{33}$$

Equations (31) and (32) again give the solution at a node i,j, in terms of the four surrounding nodes. The solution is again arrived at by iterating, using the Gauss - Siedel method.

BOUNDARY CONDITIONS

The boundary conditions imposed at the device boundaries, can be split into two types. Dirichlet boundary conditions (fixed) are applied at ohmic contacts, and Neumann boundary conditions (derivative) are imposed at all free surfaces.

At ohmic contacts charge neutrality must exist and

thermodynamic equilibrium is imposed, leading to :

at n ohmics

$$n = \frac{(\Gamma^2 + 4n_i^2)^{1/2} + \Gamma}{2}$$

$$p = \frac{n_i^2}{\Gamma}$$

at p ohmics

$$p = \frac{(\Gamma^2 + 4n_i^2)^{1/2} + \Gamma}{2}$$

$$n = \frac{p_i^2}{\Gamma} \tag{34}$$

the boundary conditions on potential at a contact are given in terms of the quasi-Fermi level :

$$\phi_{ni} = Vapp_i$$
$$\phi_{pi} = Vapp_i \tag{35}$$

where i is the contact number

At free surfaces the perpendicular field is set to zero

$$\frac{\partial \psi}{\partial \hat{n}} = 0.0 \tag{36}$$

also the perpendicular current is set to zero

$$\frac{\partial Jn}{\partial \hat{n}} = \frac{\partial Jp}{\partial \hat{n}} = 0.0 \tag{37}$$

The contact currents are evaluated by integrating the perpendicular current on a path around the contact

$$I = \int_p (\vec{J}_n + \vec{J}_p) . ds \tag{38}$$

SIMULATION RESULTS

The planar device structure analysed in this paper, is considered to be a simplification of the mesa structures that are most commonly fabricated. The HBT is a vertical device, the dimensions of which are dependent on the crystal growth technique being used.

Junctions grown by MBE can be as abrupt as a single mono-layer, (few Å) and indeed junctions are often grown to such limits. For this reason the doping profile modelled in the HBT is as shown in figure 4, being very simple when compared to those in diffused transistors. The P^+ base
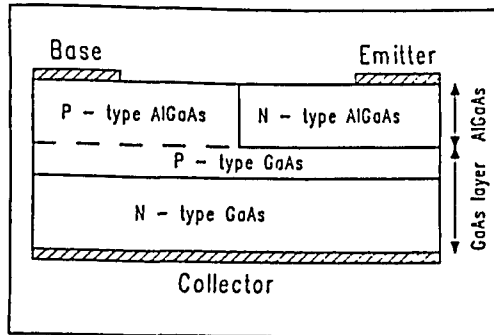
Figure 4.

Device geometry.

contact region is produced by implanting into the AlGaAs emitter layer, and the side walls of the implant are assumed to produce an abrupt PN AlGaAs homojunction. When biasing such a structure, it might well be expected that the current injection across this junction will dominate the device characteristics; however this is not the case since the GaAlAs homojunction has a higher built - in potential than the pN heterojunction, and so does not turn on as early. The collector contact is along the bottom of the device, it is felt that this simplification is justified, since the collector contact doping level is very high and will have little effect on the contact currents. There are usually two base contacts in a device of this type, the whole structure being symmetrical around the centre of the emitter metalization, but by simulating only half of the device, the run time and memory requirements will be halved, without any loss of information. The aluminium mole-fraction profile at the emitter-base junction is extremely important in the design of HBT's. For example, the turn-on voltage experienced in the transfer characteristics of the HBT is attributable to the difference between the emitter and collector built-in potentials. The existance of a turn-on voltage is highly undesirable when designing digital circuits, as higher power dissipation will result. One can control the turn-on voltage to some extent by careful design of the aluminium grading profile.

Figure 5(a) shows the result of simulating a 1-dimensional pN heterojunction, at zero bias. The p-type (GaAs) doping is 10^{18}/cm^3, whilst the n-type (Al sub 0.3 Ga sub 0.7 As) doping is 2×10^{18}/cm^3. Figure 5 (b) shows the associated aluminium profile, which is essentially abrupt (10
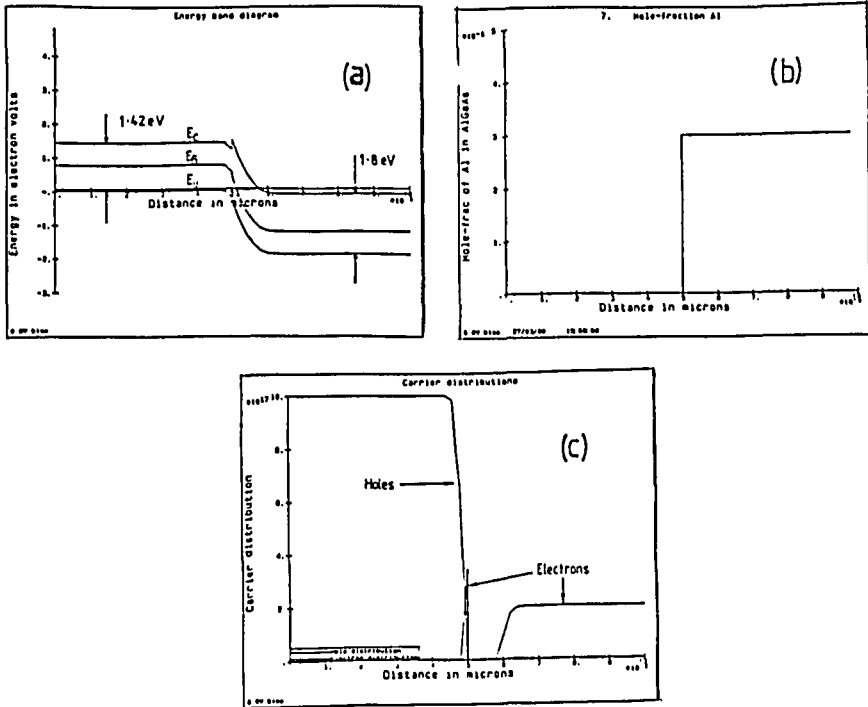
Figure 5.

1-D Abrupt heterojunction simulation (a) Energy-band diagram,
(b) Aluminium mole-fraction, (c) Carrier distributions.

Å). The formation of a "spike" and a "notch" in the
conduction band can be seen clearly, with an associated
accumulation of electrons at the notch (figure 5 (c)). The
notch in the conduction band will produce a trapping centre
where recombination will be high. It should also be noted
that the intrinsic Fermi-level is discontinuous at the
heterointerface, this is a result of the fact that the
conduction band edge depends on the assumptions of equations
(11) and (12), that is that it depends on the difference in
electron affinities.

Figure 6 shows a junction with the same doping profile as
in the previous example, however, the aluminium is graded over
500Å, from the interface into the n-type region. The spike at
the interface is lowered by 0.307 eV, this will mean higher
electron injection levels, and so higher gain transistors.
I-V characteristics for the graded (500 Å) and the abrupt (10
Å) diodes are shown in figure 7
These plots demonstrate that the current is higher for a given
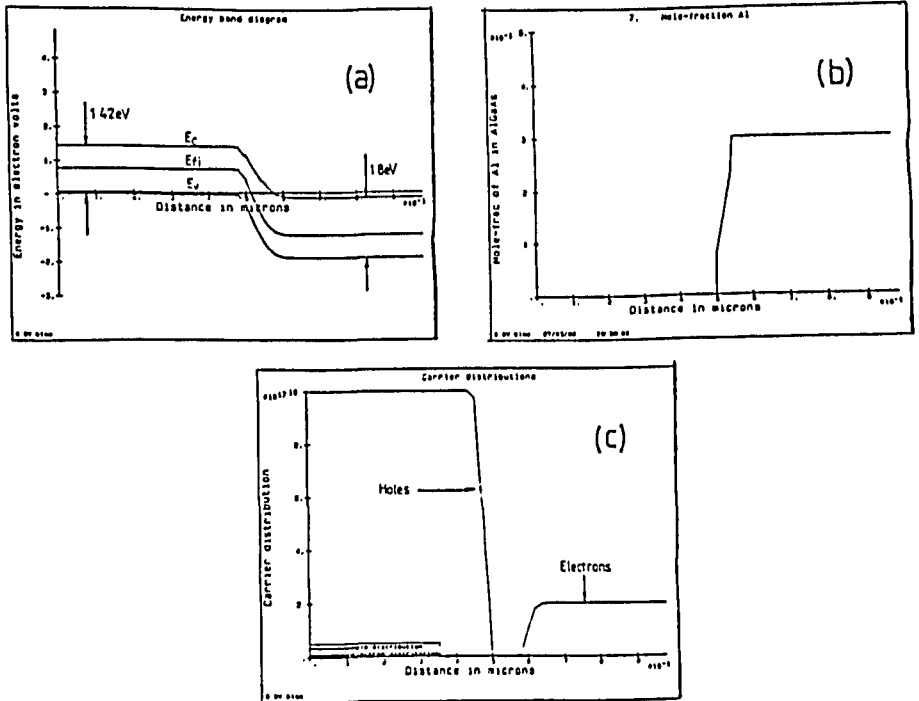bias, with the graded junction than it is for the abrupt

Figure 6.

1-D Graded heterojunction simulation   (a) Energy-band diagram,
   (b) Aluminium mole-fraction, (c) Carrier distributions.

junction. One can explain this by looking at the energy-band
diagrams of figures 5 and 6; the spike in the abrupt case
rises up above the conduction band edge in the p type material
when the junction is forward biased, thus maintaining a high
barrier for electrons to be injected over. This barrier does
not exist when the aluminium composition is graded, and the
electron injection level does not suffer the same reduction.
Also included in Figure 7 is the curve for a homojunction for
comparison, the current is higher than for both heterojunction
cases as holes are not prevented from taking part in the
conduction.

The finite difference grid used in the simulation of an
HBT is shown in figure 8. The transistor is 1.2µm deep by
4.0µm long, both emitter and base contacts are 1.0µm.
Figure 9 shows the doping profile used in this transistor
simulation, on a logarithmic scale (negative values correspond
to a net acceptor level). It can be seen that the grid lines
become far more closely packed in the vicinity of junctions,
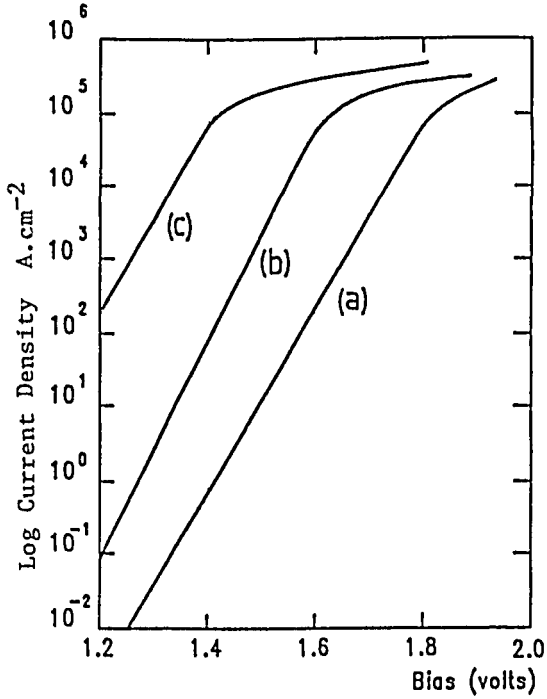this is because the potential varies much more rapidly in

Figure 7.

I-V characteristics of a pN heterojunction having
different grading profiles (a) abrupt (b) linear
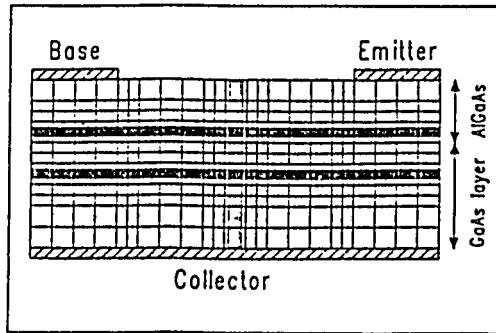grading over 500 Å (c) homojunction.

Figure 8.

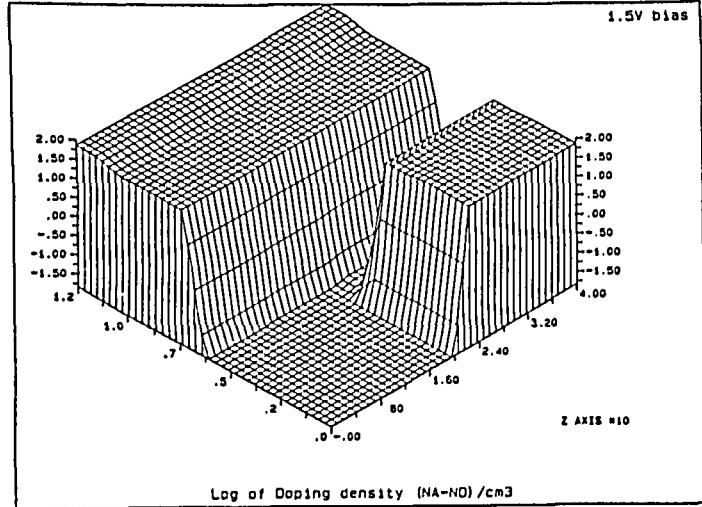Finite-difference grid used in simulation.

Figure 9.

Doping profile.

these regions. The error is also reduced in these regions by using the smaller step sizes. Imposing a bias of 1.5V at the base-emitter junction and 0.0V across the base-collector gives the potential distribution in figure 10.
It can be seen that there is a barrier in the base region where the potential profile rises, corresponding to the p-P heterojunction. There is also a slight depletion of holes noticeable in the distribution shown in figure 11.

CONCLUSIONS

In this paper, the simulation of GaAs/AlGaAs heterostructure devices has been discussed. A simple modification to the basic "phenomenological" device equations has allowed the positional dependence of the band structure to be incorporated into a numerical model. These modifications can easily be made to device simulation codes, providing the various materials parameters are known. The model has been used to predict the I-V characteristics for a heterojunction diode, and has shown that the spike in the conduction band for the abrupt case prevents the injection of electrons. This must be taken into account in the design of heterojunction bipolar transistors in order to achieve optimum emitter efficiency. A two dimensional implementation of the model has been used to predict the behaviour of the heterojunction bipolar transistor. In the near future the model will be extended to allow analysis of the high frequency behaviour of
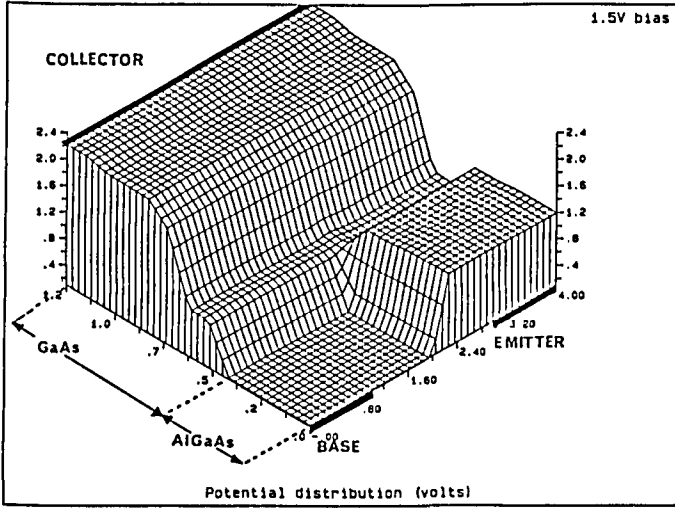
Figure 10.

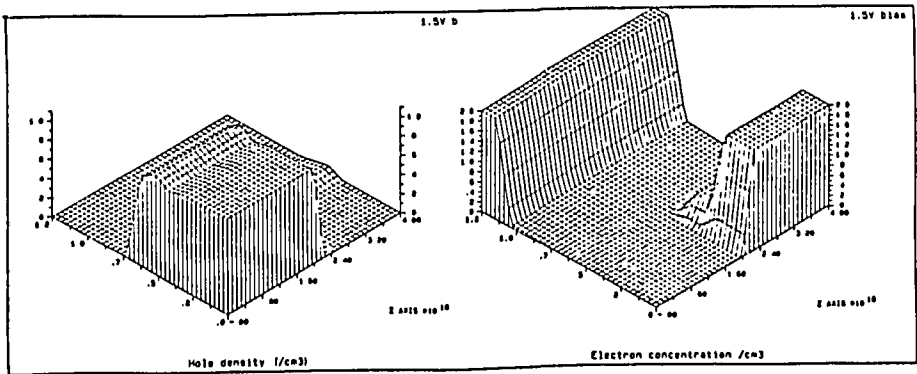Potential distribution for the HBT : V_{be} - 1.5V, V_{bc}=0.0V

Figure 11.

Carrier profiles in the HBT.

the HBT on the emitter-base grading profile.

ACKNOWLEDGEMENTS

REFERENCES

[1] Asbeck, P.M., Miller, D.L., Asatourian, R, and Kirkpatrick, C.G.
"Numerical simulation of GaAs/GaAlAs heterojunction bipolar transistors."
IEEE, Vol. EDL-3 pp 403-406 December 1982.

[2] Asbeck, P.M., Miller, D.L. et al.
"Application of heterojunction bipolar transistors to high speed, small-scale digital intigrated circuits."
IEEE, GaAs IC Symp 1984.

[3] Kim, B., Tserng, H.Q., Tiku, S.K. and Shih, H.D.
"AlGaAs/GaAs heterojunction bipolar power transistors"
Electron Lett. Vol.21 No.7 1985 pp258-259

[4] Su, L.M., Grote, N., Kaumanns, R., Katzscner, W. and Bach, H.G.
"An InGaAsP/InP double-heterojunction bipolar transistor for monolithic integration with a 1.5 μm laser diode."
IEEE, Vol. EDL-6 No.1 Jan 1985. pp14-17.

[5] Sze, S.M.
"Physics of semiconductor devices"
Pub Wiley 2nd Edn.

[6] Shockley, W.
"Electrons and holes in semiconductors"
Pub Van Nostrand Co Inc.

[7] Marshak, A.H. and van Vliet, K.M.
"Electrical current in solids with position-dependent band structure."
Solid-state Electron ., Vol. 21, pp 417-427. 1978

[8] Lundstrom, M.S. and Schuelke, R.L.
"Numerical analysis of heterostructure semiconductor devices"
IEEE Vol. ED-30 No. 9 Sept 1983 pp1151-1159.

[9]   Dingle, R., Weigmann, W. and Henry, C.H.
       "Quantum states of confined carriers in very thin
       $Al_x Ga_{1-x} As-GaAs-Al_x Ga_{x-1} As$ heterostructures."
       Phys Rev Lett., Vol. 33 pp 827-830 sept 1984.

[10]   Casey, H.C. and Panish, M.B.
       "Heterostructure lasers"
       New York: Academic 1978.

[11]   Kurata, M. and Yoshida, J.
       "Modeling and characterization for high-speed GaAlAs-
       GaAs n-p-n heterojunction bipolar transistors"
       IEEE Vol. ED-31 No. 4 pp467-473. Apr 1984.

[12]   Freeman, K.R. and Hobson, G.S.
       "The V_{FT} relation of CW Gunn Effect Devices"
       IEEE, Vol ED-19 pp62 1972.